ADVANCED OPTICAL MATERIALS
www.advopticalmat.de

Optical Anapoles: Concepts and Applications

*Kseniia V. Baryshnikova, Daria A. Smirnova, Boris S. Luk'yanchuk, and Yuri S. Kivshar**

Interference of electromagnetic modes supported by subwavelength photonic structures is one of the key concepts that underpins the nanoscale control of light in metaoptics. It drives the whole realm of all-dielectric Mie-resonant nanophotonics with many applications for low-loss nanoscale optical antennas, metasurfaces, and metadevices. Specifically, interference of the electric and toroidal dipole moments results in a very peculiar, low-radiating optical state associated with the concept of optical anapole. Here, the physics of multimode interferences and multipolar interplay in nanostructures is uncovered with an intriguing example of the optical anapole. The recently emerged field of anapole electrodynamics is reviewed, explicating its relevance to multipolar nanophotonics, including direct experimental observations, manifestations in nonlinear optics, and rapidly expanding applications in nanoantennas, active photonics, and metamaterials.

1. Introduction

During last decade, we observe a growing interest to study various optical effects associated with the so-called toroidal electrodynamics,[1] in particular, in the field of metamaterials and nanophotonics. This interest originates largely from many opportunities provided by multipolar response of subwavelength optical structures, allowing a deeper insight into many optical phenomena at the nanoscale, including multipolar nonlinear nanophotonics.[2] Conventional multipole expansions,[3–5] applied to dynamic charge–current distributions on the length scales much smaller than the effective wavelength of light, feature dominant Cartesian electric and magnetic dipoles. Nonetheless, when the area of dynamic charge–current distribution is comparable to or larger than the effective wavelength of light, higher order multipoles including dynamic toroidal multipoles become non-negligible and contribute to optical response.

The physics of interference and interplay between three families of multipolar modes:[6] electric, magnetic, and toroidal ones, underpins nanoscale light manipulation. Indeed, toroidal multipoles provide physically significant contributions to the basic characteristics of matter including absorption, dispersion, and optical activity.[1] In the far field zone, they produce the same radiation patterns as corresponding electric or magnetic multipoles. It can lead to destructive interference effects and vanishing scattering accompanied with highly nontrivial field distribution and strong light confinement. Perhaps, the simplest example of this kind is the interference of the electric dipole (ED) and toroidal dipole (TD) modes. The toroidal dipole corresponds to currents flowing on the surface of a torus. Since both EDs and TDs have identical radiation patterns, when coexcited and spatially overlapped with the same radiation magnitude but out of phase, they cancel the scattering of each other in the far field region, and the scatterer appears to be invisible. Such a radiationless state with nontrivial oscillating current configuration (in analogy with nonoscillating poloidal current) was termed anapole (from Greek "ana," "without," thus meaning "without poles"). In fact, this term, as well as toroidal moments, was first theoretically introduced by Zeldovich back in 1957,[7] and also occurs in the nuclear[8] and dark-matter physics.[9,10] In the context of classical electrodynamics, an anapole mode corresponds to a specific type of the charge–current distribution that neither radiates nor interacts with external fields. In a broader context, in the scattering theory the anapole is referred to the suppression of scattering independently of the multipoles involved.

In the subwavelength dielectric particles, the optical response is governed by the induced polarization currents which generate electric and magnetic multipoles.[11,12] Special distributions of polarization currents inside dielectric particles are capable of producing optical anapole modes.[13] Such weakly radiating modes have great potential for numerous applications in nanophotonics and metaoptics, which motivates this review. We discuss the basic properties of these special optical states, and review briefly the recent progress in the field of anapole electrodynamics with applications to nanophotonics, nonlinear optics, and metamaterials.

Dr. K. V. Baryshnikova, Prof. Y. S. Kivshar
International Research Center of Nanophotonics and Metamaterials
ITMO University
St. Petersburg 197101, Russia
E-mail: Yuri.Kivshar@anu.edu.au
Dr. D. A. Smirnova, Prof. Y. S. Kivshar
Nonlinear Physics Center
Australian National University
Canberra, ACT 2601, Australia
Dr. D. A. Smirnova
Institute of Applied Physics
Russian Academy of Sciences
Nizhny Novgorod 603950, Russia
Prof. B. S. Luk'yanchuk
Faculty of Physics
Lomonosov Moscow State University
Moscow 119991, Russia
Prof. B. S. Luk'yanchuk
School of Physical and Mathematical Sciences
Nanyang Technological University
Singapore 637371, Singapore
The ORCID identification number(s) for the author(s) of this article can be found under https://doi.org/10.1002/adom.201801350.

DOI: 10.1002/adom.201801350

The concept of anapole represents a specific example of a plethora of interference effects which can occur in subwavelength dielectric particles. During recent years, several related concepts have emerged, and they show their importance for applications of all-dielectric Mie-resonant photonics. We discuss some of those effects in the concluding section of this review paper.

2. Anapole Concept in Metaoptics

The basic physics of optical anapoles can be qualitatively explained by the Mie theory describing the light scattering by spherical particles.[3,4] Within this theory, the scattering efficiency, Q_{sca}, extinction, Q_{ext}, and other characteristics of the optical response are expressed through the electric, a_l, and magnetic, b_l, scattering amplitudes

$$Q_{sca} = \frac{2}{q^2}\sum_{l=1}^{\infty}(2l+1)\left(|a_l|^2+|b_l|^2\right) \tag{1a}$$

$$Q_{ext} = \frac{2}{q^2}\sum_{l=1}^{\infty}(2l+1)\,\mathrm{Re}\,(a_l+b_l) \tag{1b}$$

Here, the efficiencies are defined as ratios of the corresponding cross-section to the geometrical cross-section $\sigma_{geom} = \pi R^2$, where R is radius of the particle. The symbol q denotes the so-called size parameter defined as $q = 2\pi R/\lambda$, and l is the index numbering the orbital modes: dipolar $l = 1$, quadrupolar $l = 2$, octupolar $l = 3$, etc. The scattering amplitudes, corresponding to the partial spherical waves, are given by

$$a_l = \frac{F_l^{(a)}}{F_l^{(a)} + iG_l^{(a)}} \tag{2a}$$

$$b_l = \frac{F_l^{(b)}}{F_l^{(b)} + iG_l^{(b)}} \tag{2b}$$

where for the spherical nonmagnetic particle of the refractive index $n \equiv \sqrt{\varepsilon}$ in vacuum, the quantities $F_l^{(a,b)}$ and $G_l^{(a,b)}$ are defined as

$$\begin{aligned} F_l^{(a)} &= n\psi_l'(q)\psi_l(nq) - \psi_l(q)\psi_l'(nq) \\ G_l^{(a)} &= n\chi_l'(q)\psi_l(nq) - \psi_l'(nq)\chi_l(q) \\ F_l^{(b)} &= n\psi_l'(nq)\psi_l(q) - \psi_l(nq)\psi_l'(q) \\ G_l^{(b)} &= n\chi_l(q)\psi_l'(nq) - \psi_l(nq)\chi_l'(q) \end{aligned} \tag{3}$$

Here, the functions

$$\psi_l(q) = \sqrt{\frac{\pi q}{2}}J_{l+\frac{1}{2}}(q), \quad \chi_l(q) = \sqrt{\frac{\pi q}{2}}N_{l+\frac{1}{2}}(q)$$

are expressed through the Bessel and Neumann functions.[3]

First, we discuss the zeros of the electric dipole scattering defined by the condition, $a_1 = 0$. This condition corresponds to $F_l^{(a)} = 0$, and it is fulfilled along the trajectory,[14] where we

Kseniia Baryshnikova graduated with honor from the Polytechnic University of St. Petersburg in 2013. She received a Ph.D. degree in optics in 2016 from the ITMO University (St. Petersburg, Russia). Currently, she is a postdoctoral fellow at the International Research Center of Nanophotonics and Metamaterials in the ITMO University. Since 2011, she is working in the field of optics of nanostructures. Her current research interests include the multipolar analysis of optical response of nanostructures, the properties of optical anapoles, and the study of topological effects in nanophotonics, as well as tunable and active metamaterials.

Daria Smirnova received her Ph.D. degree from the Australian National University in 2016. She then worked as a Postdoctoral Fellow in Australia (Australian National University, Canberra), USA (City University of New York), and Russia (Nizhny Novgorod, Institute of Applied Physics of the Russian Academy of Sciences). Her main research interests are in the field of nanoscale nonlinear optics and topological photonics.

Yuri Kivshar received a Ph.D. degree in theoretical physics in 1984 from the Institute for Low Temperature Physics and Engineering (Kharkov, Ukraine). From 1988 to 1993 he worked at different research centers in Europe and USA, and in 1993 he settled in Australia where he established the Nonlinear Physics Center at the Australian National University, being currently Head of the Center and Distinguished Professor. His research interests include nonlinear photonics, metamaterials, and nanophotonics. He received many prestigious awards including Lyle Medal of the Australian Academy of Science, State Prize in Science and Technology (Ukraine), Lebedev Medal (Russia), Harrie Massey Medal (UK), and Humboldt Award (Germany).

should consider only those solutions with $\cos(q) \neq 0$ and $\cos(nq) \neq 0$. For nonmagnetic materials, this condition corresponds to the following equation

$$\begin{aligned} &1-n^2+q(n^2-1+n^2q^2)\cot(q) \\ &+nq(n^2-1-n^2q^2)\cot(nq) \\ &+nq^2(1-n^2)\cot(q)\cot(nq)=0 \end{aligned} \tag{4}$$

For example, at $n = 4$ the first zero is reached at $q = 1.1654$, and, as explained below, arises due to the destructive interference of the Cartesian electric and toroidal dipoles radiation.[13,14] As an example, in **Figure 1**a–c we show this "ideal anapole" which originates from the Mie theory, where the only electric dipole contribution is taken into account in the scattered field. One can easily identify the poloidal current distribution of the electric vector inside the nanoparticle in Figure 1c. However, under influence of (always present) higher-order modes, this picture becomes less ideal. This problem was discussed in ref. [14] in detail. We notice that there is almost no energy flow in the region inside the loops of the separatrices around the singular points of the Poynting vector distribution. Such an electric anapole can be considered as being equivalent to a confocal system of two lenses with the numerical aperture (NA) close to unity.[14]

In a similar way, one can find the conditions for the magnetic dipole amplitude satisfying the relation $b_1 = 0$ (the so-called magnetic anapole). There is a principal difference between energy distributions for the electric and magnetic anapole modes: while for the electric anapole the energy is trapped inside the particle on the subwavelength scale, for the case of magnetic anapole the energy is expelled outside the particle with the near-field enhancement similar to that usually associated with plasmonic particles.[14] The so-called hybrid anapole modes can be formed with simultaneous excitation of electric and magnetic anapole modes. For spherical particles, partial contributions from higher-order modes hinder this effect and pure hybrid anapole modes do not exist. Nonetheless, we expect that this restriction could be removed for other more complex geometrical shapes (disks, bricks, spheroids, etc.) or multilayered particles. Applying the same approach, the concept of anapole as nontrivial nonradiating current distributions can be generalized to any higher order expansion of the Mie theory. For example, for vanishing a_2 coefficient, an electric quadrupolar anapole is inferred as a

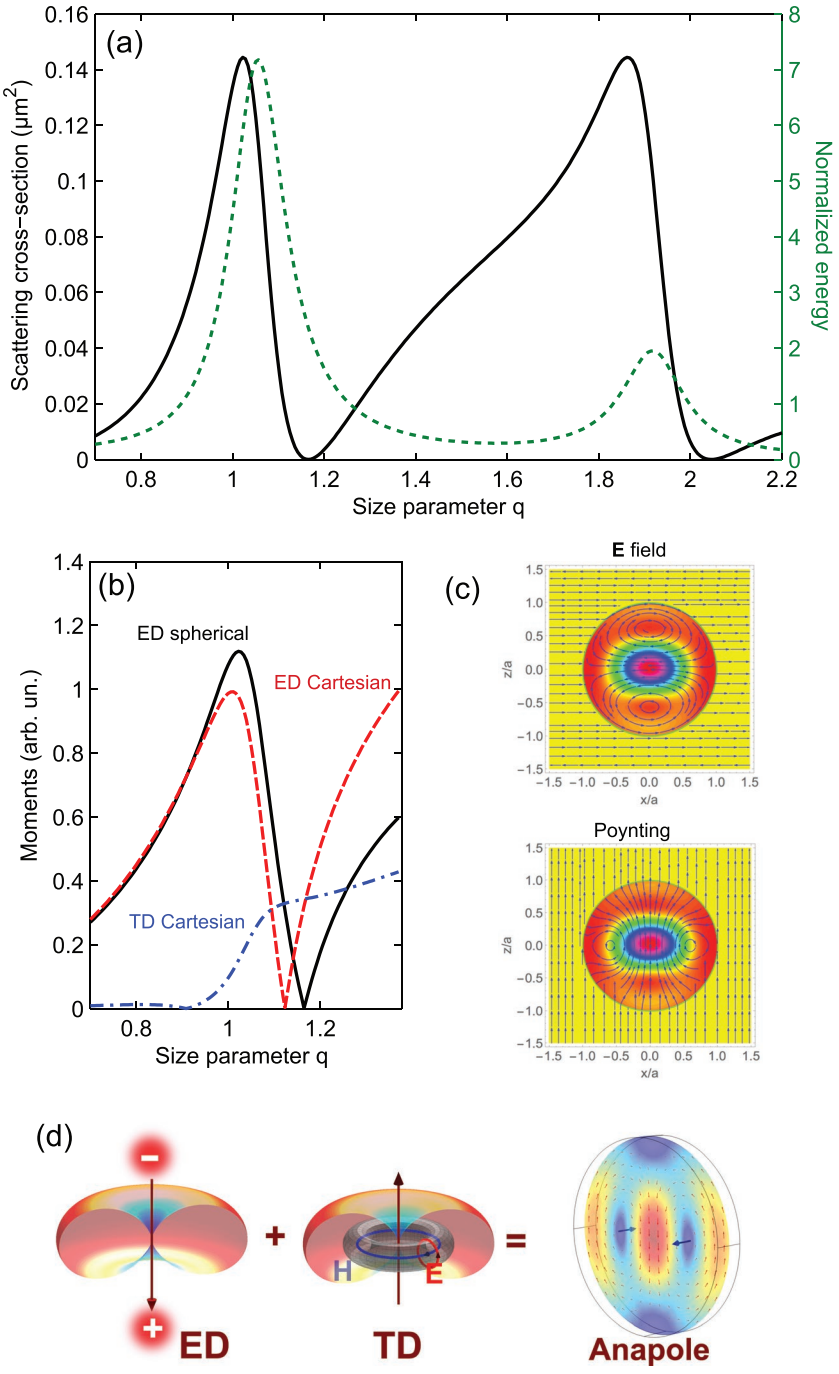

Figure 1. a) Scattering cross-section (black) and normalized time-averaged energy density (dashed green) of the electric dipole field excited inside a dielectric spherical particle of refractive index $n = 4$ at wavelength 550 nm. b) Calculated spherical electric dipole $|\mathbf{p}|$ (black), Cartesian electric $|\mathbf{p}_{Car}|$ (red) and toroidal $|-ik\mathbf{T}_{Car}|$ (blue) dipole moments for a dielectric particle of refractive index $n = 4$ in vacuum at wavelength 550 nm. c) The poloidal current distribution of the vector electric field (top) inside the particle and distribution of the Poynting vector (bottom) at $q = 1.1654$. d) Anapole concept: the destructive interference of the electric (ED) and toroidal (TD) dipole moments with identical doughnut-shaped radiation patterns and differing charge–current distributions suppresses the far-field scattering to create an optical anapole mode in the silicon nanodisk (calculated numerically for parameters of ref. [13]). The electric dipole moment is illustrated as a separation of positive and negative electrical charges. The toroidal dipole moment is associated with the circulating magnetic field **H** and poloidal electric field **E** distribution. The mode profile is shown at midheight cut of the disk.

mutual compensation of Cartesian electric quadrupole and the toroidal quadrupole modes.[17,18]

In the Rayleigh limit, any subwavelength particle effectively scatters light as an electric dipole, and the scattering increases with the fourth power of the frequency according to the well-known formula[19]

$$Q_{\mathrm{sca}}^{(\mathrm{Ra})} = \frac{8}{3}\left|\frac{\varepsilon-1}{\varepsilon+2}\right|^2 q^4 \tag{5}$$

It implies that electric dipole scattering is always present. However, by employing subwavelength particles with high values of the refractive index, it is possible to suppress the scattering below the Rayleigh approximation with the anapole mode excitation.[20] The scattering diagram of particles sustaining the anapole mode has no rotational symmetry, that implies polarization-dependent scattering (excepting scattering in the backward and forward directions).[20,21] Similar behavior of the directivity changing in the vicinity of quadrupole resonance within weakly dissipating plasmonic particles was described in ref. [22]. Though the spherical geometry permits suppressing the electric and magnetic dipole moments, it does not allow implementing the same with the quadrupole and octupole modes simultaneously. Nonetheless, by using nonspherical geometries or layered structures, simultaneous suppression of higher-order multipolar contributions could be achieved. For example, it is possible to minimize the scattering cross section of spheroidal[23] or disk-shaped particles.[13] Practical applications of optical anapole structures are mostly related to nonspherical scatterers. Design of such structures needs the multipole expansion[4] of the electromagnetic fields of a subwavelength system of charges and currents.

Multipolar decomposition can be carried out in both spherical and Cartesian bases[15,16,24–26] based on light-induced polarization or displacement current, $\mathbf{J}(\mathbf{r}) = -i\omega\mathbf{P}(\mathbf{r}) = -i\omega\varepsilon_0(\varepsilon-1)\mathbf{E}(\mathbf{r})$, where $\mathbf{E}(\mathbf{r})$ is the total electric field inside the particle. In the context of a multipole expansion, the origin of toroidal multipole moments can be understood from first principles. Exact multipolar expansion in a spherical basis does not use, contrary to the Taylor expansion in Cartesian coordinates, the approximation of small sources in the long-wave length limit. Over this approximation the derivation procedure appeals to the tensor algebra[27] and becomes more intricate, that may be a reason why toroidal multipoles were overlooked often in Cartesian Taylor expansion. With the canonical spherical basis, one can get the three multipole moment families in a more direct and natural way.[15,28] The radiated field (up to the quadrupolar order $l = 2$) is related to the induced multipole moments as

$$\mathbf{E}_{\mathrm{sca}}(\mathbf{n}) \approx \frac{k_0^2}{4\pi\varepsilon_0}\frac{e^{ik_0 r}}{r}\left([\mathbf{n}\times[\mathbf{p}\times\mathbf{n}]] + \frac{1}{c}[\mathbf{m}\times\mathbf{n}] - \frac{ik_0}{6}[\mathbf{n}\times[(\hat{Q}^e\mathbf{n})\times\mathbf{n}]] - \frac{ik_0}{2c}[(\hat{Q}^m\mathbf{n})\times\mathbf{n}] + \cdots\right) \tag{6}$$

where $\mathbf{p}$, $\mathbf{m}$, $(\hat{Q}^e\mathbf{n})$, $(\hat{Q}^m\mathbf{n})$ are the spherical multipole moments expressed in the Cartesian coordinates. The exact expressions for these moments valid for any particle's size and shape are derived in ref. [15]. The approximate Cartesian multipole moments are obtained in the long-wavelength approximation by expanding each multipole term with respect to kr in the Bessel functions entering the exact expressions, and correspond to the leading order. Thereby, the toroidal multipoles are retrieved as the next-order terms in these expansions.[15–17] In particular, we get $\mathbf{p} \approx \mathbf{p}_{\mathrm{Car}} + ik\mathbf{T}_{\mathrm{Car}}$, where Cartesian electric dipole $\mathbf{p}_{\mathrm{Car}}$ and toroidal dipole $\mathbf{T}_{\mathrm{Car}}$ moments are given in **Table 1**, where $j_{1,\,2,\,3}$ is spherical Bessel function of the first, second, and third order, respectively, and integration is performed over the nanoparticle volume. Neglecting higher-order terms, including mean-square radii multipoles $\mathbf{m}^{(1)}$ and $\mathbf{T}^{(1)}$,[16,29] the scattering cross-section in vacuum can be then approximately calculated using Cartesian moments as[24]

$$\sigma_{\mathrm{sca}} \approx \frac{k_0^4}{6\pi\varepsilon_0^2\,|\,\mathbf{E}_{\mathrm{inc}}\,|^2}\left|\mathbf{p}_{\mathrm{Car}} + ik\mathbf{T}_{\mathrm{Car}}\right|^2 + \frac{k_0^4\mu_0}{6\pi\varepsilon_0\,|\,\mathbf{E}_{\mathrm{inc}}\,|^2}|\,\mathbf{m}_{\mathrm{Car}}\,|^2 + \frac{k_0^6}{720\pi\varepsilon_0^2\,|\,\mathbf{E}_{\mathrm{inc}}\,|^2}\sum|\hat{Q}^e_{\mathrm{Car}}\,|^2 + \frac{k_0^6\mu_0}{80\pi\varepsilon_0\,|\,\mathbf{E}_{\mathrm{inc}}\,|^2}\sum|\hat{Q}^m_{\mathrm{Car}}\,|^2 + \cdots \tag{7}$$

The fundamental character of toroidal moments seems to be questionable in electrodynamics, as they mathematically appear as terms in series expansions. However, toroidal moments are a useful concept for describing certain charge–current distributions. Remarkably, three families of multipoles are complementary because they represent distinct physical symmetry properties.[28] For instance, for dipole moments: $\mathbf{p}_{\mathrm{Car}}$ appears even under time reversal, while odd under spatial inversion, $\mathbf{m}_{\mathrm{Car}}$ is odd under time reversal, but even under spatial inversion, and $\mathbf{T}_{\mathrm{Car}}$ turns odd under both time and spatial inversion.

Thus, the first zero of the electric dipole scattering by a spherical particle, for example, can be explained in terms of destructive interference of Cartesian electric and toroidal dipoles, as shown in Figure 1. For small particles, electric dipoles obtained in spherical and Cartesian bases are almost identical and the toroidal moment is negligible, whereas for larger particles, whose size is comparable to the light wavelength in the medium, the toroidal dipole moment has to be taken into account (see Figure 1b). The dynamic anapole state corresponds to the vanishing spherical electric dipole, where the Cartesian electric and toroidal dipoles cancel each other, $\mathbf{p}_{\mathrm{Car}} = -ik\mathbf{T}_{\mathrm{Car}}$. In the static case $k \to 0$, when the electric dipole moment disappears, the static anapole turns synonymous to the static toroidal dipole proposed by Zeldovich.[7] At the same time, the electromagnetic energy inside the particle is not zero, implying that there exists some nontrivial excitation, see Figure 1. A similar example of the fundamental anapole state composed of a toroidal dipole moment and electric dipole moment excited in the dielectric nanodisk is shown in Figure 1d. The series of zeroes in electric dipole scattering coefficient in Figure 1a can be treated as anapoles of the increasing order, but for higher-order anapoles additional terms beyond the toroidal dipoles in the expansions of multipolar moments are required.[15,16,26]

Generally, the nontrivial solutions for the absence of radiated electromagnetic fields correspond to destructive interference between different multipole modes. They can be deduced in a similar manner to the fundamental anapole condition but by involving higher-order terms in the multipole expansion. The different multipolar terms can have the same far-field radiation

Table 1. Expressions for exact spherical and Cartesian dipole moments.[15–17]

$l=1$	spherical	Cartesian
ED	$\mathbf{p}=-\frac{1}{i\omega}\left\{\int \mathbf{J} j_0(kr)d^3\mathbf{r}+\frac{k^2}{2}\int(3(\mathbf{r}\cdot\mathbf{J})\mathbf{r}-r^2\mathbf{J})\frac{j_2(kr)}{(kr)^2}d^3\mathbf{r}\right\}$	$\mathbf{p}_{\text{Car}}=-\frac{1}{i\omega}\int \mathbf{J}d^3\mathbf{r}$
	$\approx \mathbf{p}_{\text{Car}}+ik\mathbf{T}_{\text{Car}}+\frac{k^2}{10}\mathbf{T}^{(1)}+\cdots$	$\mathbf{T}_{\text{Car}}=\frac{1}{10c}\int((\mathbf{r}\cdot\mathbf{J})\mathbf{r}-2r^2\mathbf{J})d^3\mathbf{r}$
		$\mathbf{T}^{(1)}=\frac{1}{28c}\int r^2(3r^2\mathbf{J}-2(\mathbf{r}\cdot\mathbf{J})\mathbf{r})d^3\mathbf{r}$
MD	$\mathbf{m}=\frac{3}{2}\int[\mathbf{r}\times\mathbf{J}]\frac{j_1(kr)}{kr}d^3\mathbf{r}$	$\mathbf{m}_{\text{Car}}=\frac{1}{2}\int[\mathbf{r}\times\mathbf{J}]d^3\mathbf{r}$
	$\approx \mathbf{m}_{\text{Car}}-\frac{k^2}{10}\mathbf{m}^{(1)}+\cdots$	$\mathbf{m}^{(1)}=\frac{1}{2c}\int r^2[\mathbf{r}\times\mathbf{J}]d^3\mathbf{r}$

pattern, though their relative contributions scale differently as the wavelength changes.[30,31] In particular, the lowest-order magnetic nonradiating source is formed by a magnetic dipole and its first mean-square radius (see Table 1), while toroidal multipoles can interfere with their own mean-square radii, leading to the anapole state formation even in the absence of electric multipoles.

As an alternative to the toroidal approach and multipolar decomposition, the formation of anapole states in pure dielectric nanoparticles can be described in terms of the resonant-state expansion. In this way, the anapole behavior can be interpreted as a result of a Fano-type interference between different resonant modes with complex eigenfrequencies.[32,33] The excitation of an anapole mode is associated with the characteristic Fano lineshape in the spectrum.[20] The high-order radiation-less states can be also deduced as the result of a complex interaction among the resonances (modes) of the cavity and the surrounding environment, which are mutually coupled by boundary terms, by applying a Fano-Feshbach projection scheme,[34] a theoretical method widely used in quantum mechanics of open systems.

3. Experimental Observations

The anapole mode in optics can be viewed as an engineered superposition of toroidal and electric or magnetic multipoles, resulting in destructive interference of the radiation fields. The toroidal modes involved into interference can be generated in specifically designed composite metamaterials,[1,35–43] where the near-field coupling between the individual particles' modes is capable of suppressing all standard multipoles with the electromagnetic scattering due to the resulting toroidal excitations being a dominant physical mechanism of the metamaterial response. Selective excitation of toroidal multipoles needs accurate engineering of the structure to match the specific near-field current distributions. Particular designs were proposed and fabricated that experimentally verified the anapole states in microwave metamaterials[44] and metamolecules,[45] as well as at optical frequencies.[17] Still, even simple homogeneous dielectric particles with Mie resonances can support toroidal dipole moments, coexciting with the electric and magnetic multipoles.

To observe a pure optical anapole, e.g., based on ED and TD, besides the proper excitation of ED and TD modes, the suppression of other multipoles is required. In the discussion above we considered a hypothetical situation of single partial spherical wave excitation, which is quite difficult to realize in practice. It is not possible to detect the anapole mode in homogeneous spheres with incident plane waves since the MDs and other quadrupolar excitations at the ED–TD scattering cancellation point are non-negligible. However, under proper excitation, the anapole state can be generated even in simple isolated scatterers, such as dielectric spheres, disks, nanorods.[46] Specifically, the pure anapole modes can be excited while other multipoles are suppressed using the following approaches in the optical range: i) excitation of all-dielectric particles of cylindrical, parallelepipedal, spheroidal, or other nontrivial shape with plane waves;[13] ii) excitation of all-dielectric spheres with specifically engineered wave beams (e.g., two radially polarized beams being of the same intensity but out-of-phase and counter-propagating);[47] and iii) core–shell metal–dielectric nanospheres[43] or nanorods[48] and homogeneous spherical particles possessing the radial anisotropy[49,50] with incident plane waves. Excitation of anapole modes in silicon nanoparticles can be facilitated by using structured light.[51] Particularly, azimuthally polarized focused beams can be employed to achieve the magnetic anapole modes corresponding to the suppression of magnetic dipole scattering.

First direct demonstration of the anapole state in the standalone dielectric nanoparticle was performed in 2015.[13] The first-order electric anapole, induced by the superposition of the electric and toroidal dipoles, was observed by SNOM measurements. By employing the multipole decomposition, it was numerically found that by changing the aspect ratio of a silicon nanodisk it is possible to detune all higher order multipoles away from the anapole excitation condition. Thus, for the optimized aspect ratio a silicon nanodisk exhibits a profound dip in the far-field scattering, which is accompanied by a near-field enhancement inside and around the disk (see **Figure 2**a), associated with the anapole mode configuration. Experimentally, anapole was excited in a silicon nanodisk with a height of 50 nm and diameter 310 nm, which were fabricated on a quartz substrate using standard nanofabrication techniques. The disk becomes nearly invisible in the far-field at the wavelength of the anapole mode 640 nm. Both, near- and far-field measurements confirm the anapole mode excitation in the visible spectrum range (see Figure 2a). Here the anapole wavelength is far away from resonances and destructive interference between electric and toroidal dipoles happens in the local minimum of the electric dipole moment.

Higher-order anapoles in the near infrared wavelength range were also later observed with silicon disks. The disks of 80 nm thickness and diameters varied from 470 to 970 nm were fabricated on a fused silica substrate.[26] In addition to the total scattering drops and local maxima in the accumulated electromagnetic energy, the anapole states were experimentally found to be characterized by a reduction of the normal near-field electric

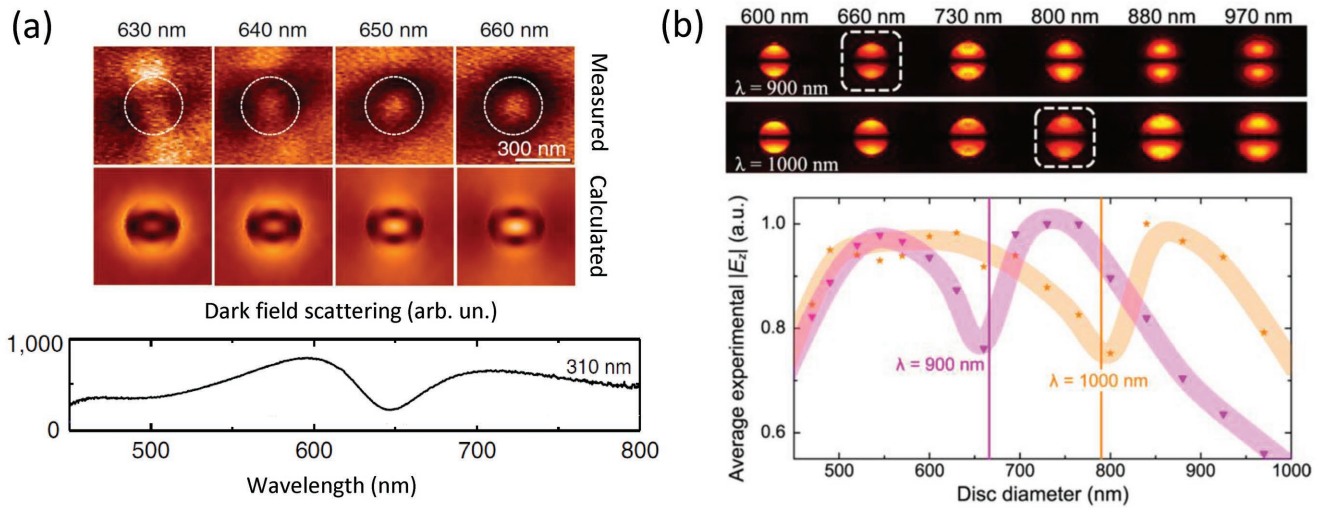

Figure 2. Experimental observation of anapole states in all-dielectric nanoparticles. a) Experimental dark field scattering spectrum of a silicon nanodisk with a height of 50 nm and a diameter 310 nm. The top row shows experimental near-field scanning optical microscope (SNOM) measurements of the near-field enhancement around the silicon nanodisk close to the anapole wavelength of 640 nm. White dashed lines in the experimental images indicate the disk position. Adapted under the terms of a Creative Commons Attribution 4.0 International License.[13] Copyright 2015, Macmillan Publishers Limited. b) Near-field detection of anapole states. Experimental near-field $|E_z|$ distribution (top) and its average value for silicon disks, measured at two different illumination wavelengths: 900 (magenta triangles) and 1000 (orange stars) nm, disk diameters are labeled on top. The disks with the lowest near-field amplitude, encircled with the white dashed lines and marked by the vertical lines, support the second-order anapole states. Adapted with permission.[26] Copyright 2017, American Chemical Society.

component and this property was successfully applied to detect the first two anapole states, as shown in Figure 2b. All three identification techniques provided similar results with deviations less than 5%. The higher-order anapole states were shown to possess stronger energy concentration and narrower resonances, which is advantageous for their applications.

Remarkable process of an active switching between dark (anapole) and bright (electric dipole) modes was demonstrated experimentally in the groups of Qiu and Bozhevolnyi.[52] $Ge_2Sb_2Te_5$ (GST) with different degree of crystallinity allows tunability of the refractive index, and thus shifting positions of resonances supported by the nanoparticle in the broadband wavelength range. It was shown that increasing of the percentage of crystalline phase in a 450 nm radius-nanosphere from 0% to 25% leads to switching the electromagnetic response of the nanosphere from the electric dipole to the anapole state. Nanodisks made of GST were fabricated by using electron-beam lithography, magnet sputtering deposition, and standard lift-off process. Then higher-order anapole states in the nanodisks were experimentally identified, suggesting much richer switching phenomena compared to the case of a symmetric GST sphere. A broadband response of the switching effect was examined and it was shown that the ED-to-anapole transition in a GST nanodisk of arbitrary cristallinity can be achieved by simply introducing a phase change $C = 50\%$ at any given wavelengths between 3.9 to 4.6 μm.

4. Applications of the Anapole Concept

4.1. Enhanced Nonlinear Effects

Engineered anapole states correspond to the cancellation of the far-field radiation in the first order and, consequently, to the energy concentration in the subwavelength volumes, as was measured experimentally in ref. [53]. A tight field confinement associated with optical anapole modes can be utilized for enhancing nonlinear interactions at the nanoscale.

The anapole state was first employed by Grinblat et al.[54] for the efficient frequency conversion in Ge nanodisks. A pronounced dip was observed in the scattering cross section, while the electric field energy is concentrated inside the dielectric disk due to the anapole mode confinement. The dependencies of the third-harmonic signal on the nanodisk size and pump wavelength were investigated. The anapole mode excited at the wavelength 1650 nm was demonstrated to boost THG conversion efficiency of 0.0001%, which by four orders of magnitude exceeds the THG in unstructured Ge reference film. Moreover, nonlinear conversion via the anapole mode was more efficient than that via the radiative dipolar resonances with increasing of THG efficiency by about one order of magnitude, implying that the anapole-induced radiation suppression in this case plays a crucial role.

The THG conversion efficiency can be further enhanced by the geometry optimization.[55,56] For example, in a metal–dielectric nanostructure composed of a Si nanodisk as a core and a gold ring as a shell, THG conversion efficiency via the anapole state reaches 0.007% at the third-harmonic wavelength of 440 nm (see **Figure 3**b). Specifically, in this geometry a Si disk plays the role of the nonradiating particle with the anapole-induced enhancement of the field, and the gold ring boosts the electric field enhancement inside the Si nanodisk due to its plasmonic properties. Similarly, in the work by the Celebrano et al.[56] hybrid metal–dielectric structures were studied experimentally as efficient frequency converters. AlGaAs nanopillar surrounded by a gold ring supports the anapole mode, consisted of equal electric dipole response of the ring and toroidal response of the pillar. This enables the improvement of both

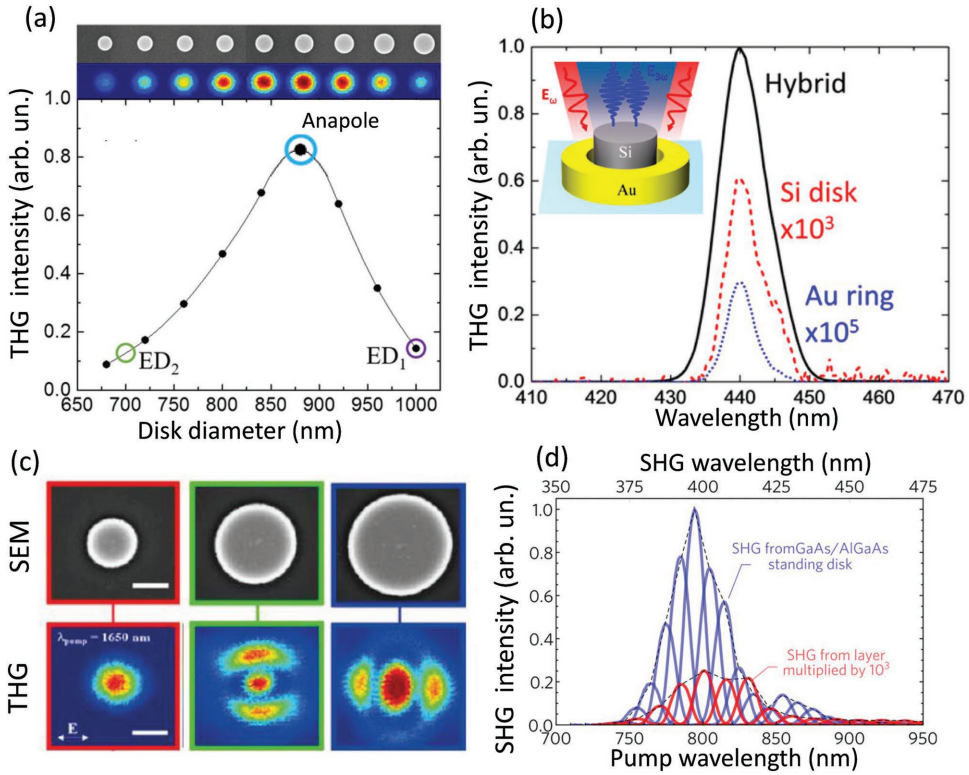

Figure 3. Nonlinear effects driven by the anapole states. a) Measured THG intensity with varying the disk diameter at the pump wavelength 1650 nm. The solid line connecting the dots is a guide to the eye. The corresponding SEM and THG intensity maps are displayed on the top. b) THG spectra of the hybrid metal–dielectric structure (shown in the inset), isolated Si nanodisk, and bare Au nanoring measured at 1320 nm excitation wavelength and 1 μW excitation power. c) SEM micrographs (top) and THG images (bottom) of Ge nanodisks with radii 350 nm (left), 550 nm (middle), and 700 nm (right). from left to right: the anapole state, the higher-order anapole, the nonanapole state. White scale bars marks 500 nm length. d) Wavelength dependence of the SHG spectra from the GaAs/AlGaAs disk (blue lines) and epitaxial layer (red lines, signal is multiplied by 10^3), the dashed gray lines are the SHG spectra envelopes; recorded by sweeping the excitation laser wavelength from 690 to 900 nm with 10 nm step. Adapted with permission.[54,55,57,58] Copyright 2015, 2016, 2017, 2018, American Chemical Society.

the second- and third-order nonlinear efficiencies, with measured enhancement factors of about 30 and 15 for the second and third harmonics generation processes, respectively.

Grinblat et al.[57] studied the effect of the high-order anapoles on the THG intensity, and compared the anapoles of different orders. They used arrays of Ge nanodisks with different radii from 300 to 700 nm keeping the fixed disk height equal to 200 nm. This allowed scanning the modes excited in the nanodisk and alongside changing the distribution of the electromagnetic fields inside the nanoparticles. In the nanodisk with the radius 350 nm at the wavelength 1650 nm, Grinbrat et al. observed the first-order (fundamental) anapole state with a typical distribution of electromagnetic fields similar to those in Figure 3c and discussed above. In the nanodisk of radius 550 nm, they observed the generation of a second-order anapole state discussed previously in ref. [26]. THG efficiencies from the anapole states of the first- and second-orders were compared to each other and to that from a 700 nm radius nanodisk. The latter has quite similar distribution of electromagnetic fields inside the nanoparticle (see Figure 3c) but it corresponds not to a minimum but to a maximum of the overall extinction. THG from all those modes was measured at the pump wavelength 1650 nm. It was established experimentally that the third-harmonic intensity is higher by orders of magnitude in the case of the second-order anapole state, being in agreement with results of ref. [26] and suggesting that the energy concentration increases as the anapole state order grows. As a result, high THG conversion efficiency of up to 0.001% to the wavelength of 550 nm was achieved.

Efficiency of THG can be also significantly increased by placing a dielectric anapole resonator on a metallic mirror. Xu et al.[59] demonstrated experimentally that this can enhance the third-harmonic radiation intensity by additional two orders of magnitude compared to a typical anapole resonator located on an insulator substrate.

While silicon is a centrosymmetric material and possesses strong cubic nonlinearity, its quadratic nonlinearity is inhibited in the bulk and second-harmonic generation (SHG) can be generated mostly from the interfaces. For efficient second-order nonlinear applications, nanostructures made of high-permittivity noncentrosymmetric dielectric materials, such as $A_{III}B_V$ semiconductors, can be advantageous. In ref. [58] SHG intensity at the anapole state in the geometry of vertically standing GaAs/AlGaAs pillars on a substrate was demonstrated to exceed that in the bare layer up to 5 times (see Figure 3d). Rocco et al.[61] studied the effective coupling of electric and toroidal modes in AlGaAs nanodimers to enhance the SHG efficiency with respect to the case of a single isolated nanodisk. They have demonstrated that proper near-field coupling can

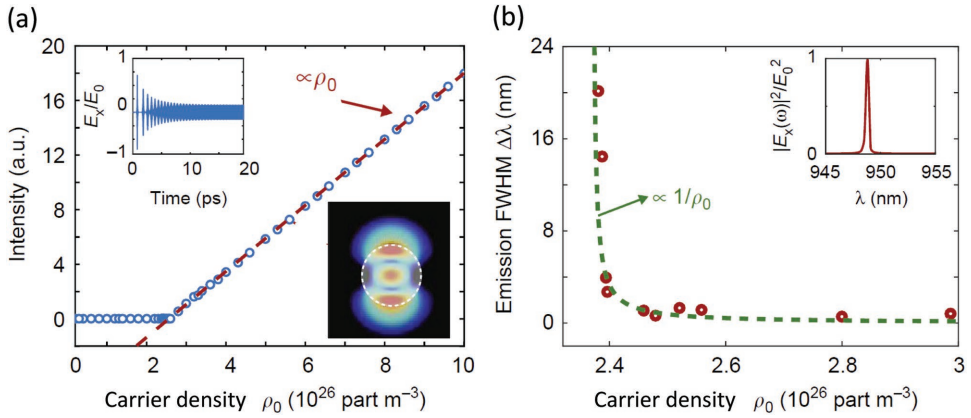

Figure 4. Operation of the anapole nanolaser. a) Input/output diagram of anapole amplitude versus carrier density ρ_0. Upper inset: time trace of the field component E_x. Lower inset: cross-section of the electromagnetic energy in the steady-state. b) Corresponding linewidth behavior and (inset) power spectral density measured inside the nanodisk. Adapted with permission.[60] Copyright 2017, Springer Nature.

provide further degrees of freedom to control the polarization state and the radiation diagram of the second-harmonic fields.

Similarly, the anapole state can enhance other nonlinear processes, in particular, the Raman response of Si nanoparticles, as shown recently both theoretically and experimentally.[62] The Stokes and anti-Stokes Raman spectra from Si nanoparticle arrays with varying disk radius were collected using excitation at 785 nm wavelength. A pronounced phonon peak was observed at 522 cm^{-1}. For silicon nanocylinders with radius of 190 nm, the Stokes emission shows the largest enhancement of more than 80 times as compared to an unstructured silicon film. These nanodisks sustain the anapole mode at the pump wavelength, manifested as minima in extinction and reflectivity.

4.2. Nanolasers in Subwavelength Photonics

The concept of coherent light emitters with the nanoscale sizes has attracted a lot of attention especially during last decade due to the recent technological progress in lab-on-chip fabrication technologies. Nanolasers are usually associated with plasmonics where the subwavelength localization of light is driven by the physics of surface plasmon polaritons. Such spaser-type nanolasers have been fabricated and studied experimentally.[63,64] Dielectric photonic structures have advantages due to low ohmic losses of dielectric materials, but they usually require much larger scales such as those provided by semiconductor nanowires.[65,66] Application of anapoles to the physics of nanolasers looks especially attractive because such states do not dissipate energy in the far-field region and effectively accumulate energy inside the nanoparticle, which can increase the local state density and subsequently enhance the overall laser efficiency. By harnessing the nonradiating nature of the anapole state, one can engineer nanolasers as on-chip sources with unique optical properties.

Recently suggested an anapole nanolaser[60] is based on a tightly confined anapole mode produced by interference of the dipole mode and toroidal mode in an optically pumped semiconductor nanodisk (see also refs. [67,68]). Importantly, anapole modes can be used to realize efficient coupling of light with nanostructures, which is one of the challenges in modern nanophotonics. Indeed, in ref. [60], Gongora et al. studied an advanced theoretical model of spontaneously polarized nanolaser. In the proposed structure light is coupled into waveguide channels, with peak coupling intensity ten thousands larger than that for classical nanolasers. Moreover, the anapole nanolaser allows generating ultrafast (of 100 fs) pulses via spontaneous mode locking of several anapole modes. The anapole laser does not require extended structures and the radiationless state is excited with no additional radiating components. A resonator employing the anapole mode is based on InGaAs semiconductor.

Figure 4a,b shows the characteristics of the electromagnetic field amplification (namely, linewidth and intensity) in the nanodisk laser of $In_{0.15}Ga_{0.85}As$ with diameter 440 nm and height 100 nm operating at the anapole mode. Amplified intensity depends linearly on the pumping rate (see Figure 4a,b), as typical to a standard laser (see Figure 4a). This anapole laser also possesses an equivalent Schawlow–Townes linewidth (see Figure 4b) with an asymptote of 2 nm. A typical time evolution of the electric field is displayed in Figure 4a, the upper inset, where the stable state of stationary emission is achieved after an initial transient. The corresponding intensity spectrum in the inset of Figure 4b confirms that the emission corresponds to the amplified anapole state at 948 nm. The electromagnetic field distribution in nanodisk at this wavelength is shown in the lower inset of Figure 4a. Based on such nanolaser it can be possible to construct on-chip ultrafast pulse generation due to anapole mode locking, as described in ref. [60].

Coupled anapoles can provide a new path for nonradiative energy transfer.[69,70] Due to exotic near-fields, coupling and hybridization of anapoles obey different rules compared to electric and magnetic dipoles. The *Q*-factor in nanodisk arrays can exceed that of the individual disks at the anapole mode by about ten times due to collective oscillations in arrays.[69] The coupling between the two interfering modes can be modified and *Q*-factor further enlarged by introducing a split in the disks and adjusting its gap width. Ref. [70] describes subwavelength guiding via near-field transfer of anapole states. Due to the near-field confinement produced by the anapole state, the

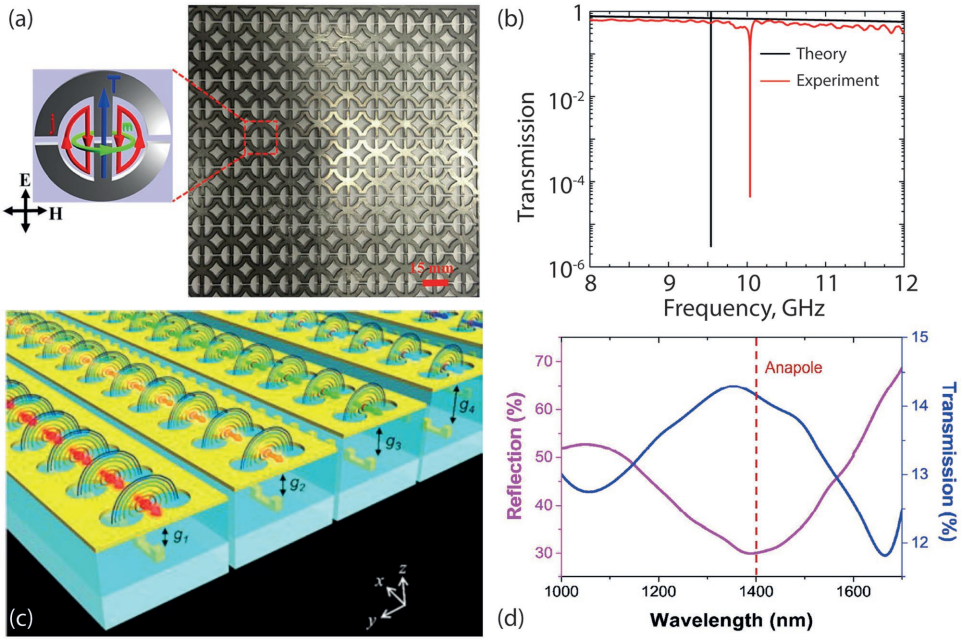

Figure 5. Designs of anapole metamaterials. a) Left: a unit cell of a metamaterial supporting toroidal dipolar excitation. Red arrows: displacement currents **j** induced by the vertically polarized plane wave, blue arrow: induced toroidal dipole moment **T** of the metamolecule, green round arrow: circulating magnetic moment **m**. Right: the metamaterial sample. b) Transmission spectra, calculated (black lines) and experimental (red lines), for the sample shown in (a). Adapted with permission.[44] Copyright 2017, American Physical Society. c) Schematic of the anapole metamaterial, consisting of a gold film perforated by dumbbell-shaped apertures, situated above a planar array of VSRRs suspended in a dielectric spacer layer. The color arrows and the streamlines show the orientation of induced toroidal dipoles and the corresponding magnetic field distribution, respectively. d) Measured far-field spectra of the plasmonic anapole metamaterial illustrated in (c) under *x*-polarized illumination. The dark-red dashed line marks the resonant wavelength of anapole mode obtained numerically. Adapted with permission.[17] Copyright 2018, American Chemical Society.

anapole nanochain appears robust against bending and splitting of the integrated waveguide. This opens a way to the realization of integrated splitters and 90° bends without parasitic radiation losses.

The insightful theoretical predictions described in this section are still to be tested experimentally.

4.3. Anapole-Driven Metamaterials

The anapole excitation has been firstly experimentally realized within engineered composite metallic metamaterials in the microwave regime, where the excitation of other multipoles is negligible.[36] In ref. [44] the electromagnetic response of the metamaterial consisting of planar conductive metamolecules formed by two symmetric split rings (see **Figure 5**a) was shown to exhibit an extremely narrow peak in transmission spectrum (Figure 5b) at the frequency where toroidal moment interferes destructively with suppression of electric dipole radiation. In ref. [17] the anapole metamaterial operating in the IR range was designed based on plasmonic nanostructures, Figure 5c. Metaatom composed of a dumbbell aperture in a gold film and a vertical split-ring resonator exhibits close to ideal suppression of electric dipole radiation. The remarkable advantage of this design is that in this structure the electric field concentrates in the imaginary torus, bounded by the dumbbell aperture, so that the area of electric field localization is accessible, which is highly relevant to sensing applications, such as the surface-enhanced Raman scattering (SERS). The efficient coupling between anapole metamaterials and molecules supporting toroidal resonances in natural substances suggests feasibility of toroidal spectroscopy. Depending on the excitation wavelength, the toroidal dipole or anapole state can be clearly identified in response spectra. At the anapole wavelength, suppression of reflection coefficient down to 30% with an increase of transmission coefficient up to 14.5% is observed experimentally, Figure 5d.

Anapoles in particles and metamolecules made of dielectric materials opens a route to low-loss metamaterials and metadevices. The feasible design of all-dielectric anapole metamaterial in the optical range was suggested theoretically ref. [71]. The proposed structure consists of arranged metamolecules—clusters of four holes perforated in a silicon slab and can be fabricated by focused ion beam techniques. The anapole state in this system corresponds to the peak up to 100% in transmission spectrum and its position depends on the parameters of the structure. Both gradual increasing an angle of illumination and reducing the depth of holes result in a redshift of transmission peak, whereas a resonance width decreases as the angle of incidence grows and, in opposite, increases with the hole deepening.

4.4. Other Applications

If scattering by some object is mainly determined by its electric dipole component, the anapole concept can be applied for cloaking of this object. For instance, if a toroidal response

of the shell can fully compensate electric dipole response of camouflaged object in the core, the overall system becomes invisible. This approach was discussed in ref. [72] theoretically with an example of a system of cylinders. The electric dipole response of a small cylinder, placed in the center of the system, can be camouflaged by the toroidal response of the shell, a cluster of four other cylinders exhibiting a strong toroidal response.

Anapole electromagnetic state can be treated as an ideal suppression of the selected multipolar order but not as a completely nonradiating source. If radiation of some multipoles is strongly suppressed, other multipoles can still radiate efficiently. In fact, at the first-order anapole, the pure magnetic dipole source can be realized, as theoretically suggested in ref. [73]. Scattering pattern of an Au core–Si shell nanodisk embedded in air with optimized dimensions was shown to approach the ideal magnetic dipole radiation pattern. Multipole decomposition proved the contributions of the electric dipole, electric quadrupole, and magnetic quadrupole to the total scattering to be negligible, while slight deviations from the ideal magnetic dipole caused by weak higher-order multipoles.

Anapole states can also be used for the formation of the electric and magnetic near-field hotspots in nanostructures. The electromagnetic energy is transformed from the far field to the tightly localized fields, thus being strongly enhanced. In ref. [53] it is demonstrated that individual all-dielectric nanostructure can trap the fields with intensity enhancement exceeding 3 orders of magnitude. This remarkable effect is achieved with a Si nanodisk supporting an anapole state by introducing a high-contrast slot area. Possibility to enhance pure magnetic hotspots with effect of spatial separation of electric and magnetic fields based on the electric dipole suppression and electric dipole enhancement was described in refs. [74–76].

The efficient excitation of nonradiating anapoles can play a significant role for enhancing light absorption in photonic nanostructures, e.g., nanodisks[77] and core–shell particles.[78] In ref. [77] the authors theoretically demonstrated wide and controllable wavelength tunability of anapole-driven absorption enhancement in dielectric nanodisks and square nanopixels, and optimum conditions to achieve the highest absorption rate on the particle sizes and excitation were identified. Thus, while for standalone germanium nanodisk absorption rate is higher than 5 in a bandwidth about 200 nm, for heterostructure combined from two different nanodisks this bandwidth is about 800 nm. The nanostructured arrays of particles were further designed to increase the absorption bandwidth that can serve as functional units in semiconductor photodetectors.

A promising application of the anapole concept can be found in the study of interaction of an anapole with molecular excitons and other molecular excitations. In the paper[82] a nanostructure consisting of silicon disk as a core and aggregate of molecules as a coaxial shell was examined. Molecules in the aggregate possess exciton excitations. The resonant coupling is proved by a peak in scattering in the vicinity of the exciton transition frequency, and two remarkable scattering dips come from a pair of eigenmodes the anapole mode splits to. These observed dips are associated with the formation of two hybrid anapole modes due to coherent exchange of energy in the heterostructure. Molecules which are located close to the apexes of the disk perpendicular to the incident polarization play the dominant role in this interaction, and a special near-field distribution characteristic to the anapole state allows increasing of the aggregate ring width and enhancement of the resonance coupling.

5. Related Interference Effects

The concept of the anapole states represents a special, yet the most intriguing, example of interference effects for isolated subwavelength dielectric particles. During recent years, several somewhat related concepts have been introduced and developed. The associated multipolar effects show their importance for numerous applications of all-dielectric Mie-resonant photonics.

The study of multipolar interference goes back to Kerker et al.[83] who considered interference between electric and magnetic dipolar modes for a hypothetical magnetic sphere. Reinvigorated by the explosive developments in the field of artificially created metamaterials over the last years, and especially by the concept of optical magnetism, the impact of the Kerker effect has intensified in the incredible way and swiftly permeated various branches of modern nanophotonics. Herewith, the concept itself has been generalized and broadened, as was described in the recent review paper,[84] not only for peculiarities in the scattering by standalone particles and arranged clusters but also for unprecedented control over transmission, reflection, diffraction, and absorption in application to metagratings and metasurfaces.

Interplay between electric and magnetic dipolar resonances makes it possible to achieve either constructive or destructive interference leading to remarkable scattering properties of subwavelength dielectric particles in the forward or backward directions.[83,84] Overlapping electric and magnetic multipoles of higher orders further suggests advanced strategies for shaping light radiation. Recently Shamkhi et al.[79] described the transverse scattering of light by high-index subwavelength particles with the simultaneous suppression of both forward and backward scattering. This unusual effect occurs when the in-phase electric and magnetic dipoles become out of phase with the corresponding quadrupoles, as shown schematically in **Figure 6**a. By applying the Mie theory, they have obtained the underlying conditions, and provided experimental data for the microwave spectral range.

Another special type of interference originates from strong coupling between the leaky modes supported by a single subwavelength high-index dielectric resonator. Rybin et al.[80] demonstrated that the strong coupling regime results in resonances with high-quality factors (Q factors), which are related to the physics of bound states in the continuum (BIC) when the radiative losses are almost suppressed due to the Friedrich–Wintgen scenario of destructive interference. One type of interfering modes is formed mainly due to reflection from a side wall of the cylinder, and they can be traced to the Mie resonances of an infinite cylinder, see Figure 6b. The other type of modes is linked to the Fabry–Perot-like resonances, so that, for a cylindrical resonator, the strong coupling between the Mie-like and Fabry–Perot-like modes is clearly manifested as avoided

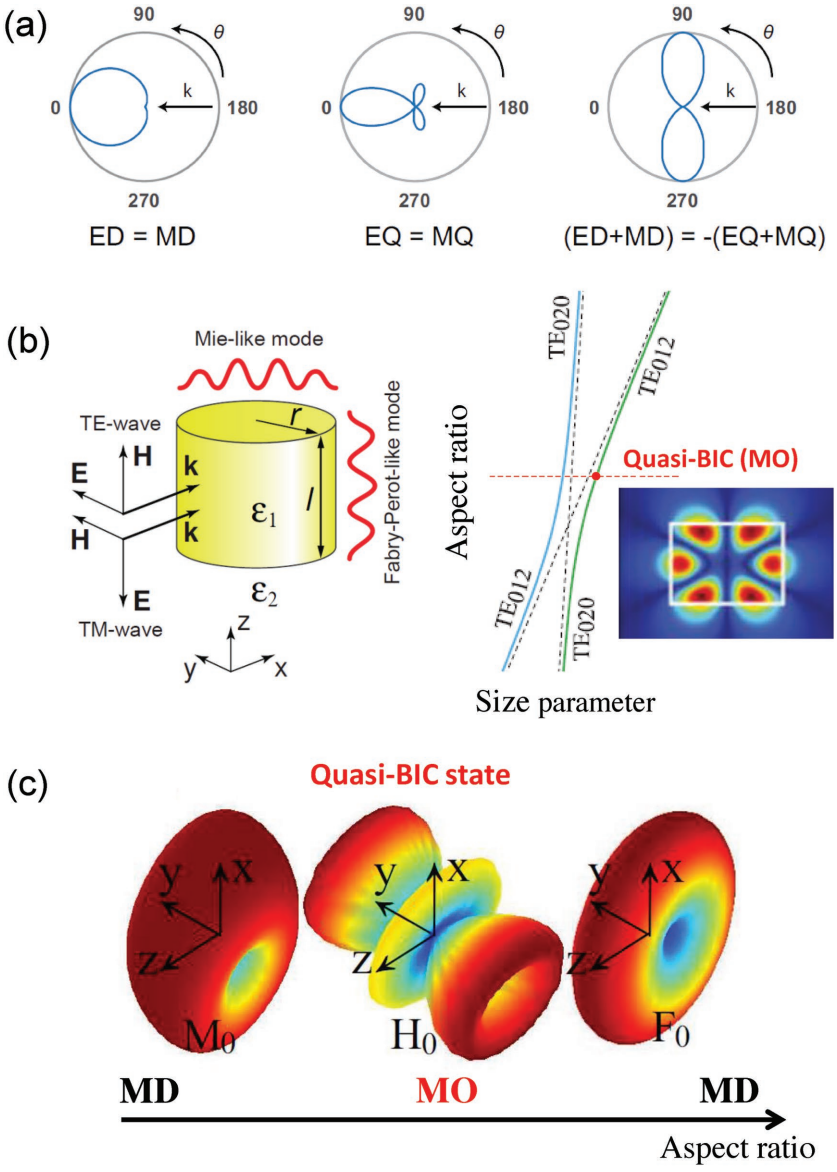

Figure 6. Examples of novel interference effects in isolated nanoparticles. a) Concept of the formation of an ideal transverse scattering pattern. Electric dipole (ED) is in-phase with a magnetic dipole (MD) and an electric quadrupole (EQ) is in-phase with a magnetic quadrupole (MQ), while the dipoles are out-of-phase with the quadrupoles. (Adapted from ref. [79].) b) Strong coupling of modes in a subwavelength dielectric resonator with an emergence of quasi-BIC state. Adapted with permission.[80] Copyright 2017, American Physical Society. c) Example of radiation pattern transformation for the mode when passing the anticrossing point. (Adapted from ref. [81].) The quasi-BIC supercavity mode condition corresponds to the magnetic octupole (MO) radiation.

resonance crossing points with the appearance of the quasi-BIC states. Additionally, Rybin et al.[80] revealed a link between the formation of the high-Q resonances and peculiarities of the Fano parameter behavior in the scattering cross-section spectra.

The formation of quasi-BICs can be naturally understood through multipolar transformations of coupled modes.[81,85] For a nonspherical shape of the resonator, the interacting modes can be in general viewed as superpositions of multipoles. For the case of Figures 6b,c, a basis of parent multipoles is constituted mainly by magnetic dipoles and octupole.

The occurrence of high-Q supercavity mode is accompanied by increasing the order of a dominating multipole from $l = 1$ (MD) to $l = 3$ (MO) and corresponds to the decoupled magnetic octupole. At quasi-BIC condition, two magnetic dipole modes interfere destructively in the coupling to the octupolar mode, thus, restoring its high quality factor.[85]

As shown in ref. [85] in the framework of the three-state model, such mutual interplay of parent multipoles essentially determines generation of both high-Q resonant states and dark states in dielectric nanoresonators. Relying on this instructive interpretation and generalized Kerker effects of interferences among different electromagnetic multipoles, the radiation of the subwavelength high-Q supermodes can be made unidirectional by breaking symmetries of the dielectric scatterers,[81] that can be useful for nanoscale lasing and sensing related applications. Similar to the anapole states, such BIC-inspired modes can be also employed for a substantial enhancement of nonlinear and quantum effects at the nanoscale.[85,86]

6. Concluding Remarks

We have presented a brief overview of the theoretical and experimental results on the rich physics of optical anapoles, putting an emphasis on the recent progress in its application to subwavelength dielectric structures and meta-optics. Being a universal physical model of nonscattering objects and nonradiating sources, the anapole mode can be accessed in nanophotonics by using conventional dielectric materials. Dielectric nanoparticles can support almost radiationless anapole modes allowing an interference of the toroidal and electric or magnetic multipoles through a geometry tuning, with a pronounced dip in the far-field scattering accompanied by the specific near-field distribution. The anapole properties, particularly, tightly confined fields, have important implications for modern nanophotonics beyond what is expected from the dipole approximation.

The anapole concept, as well as related interference effects in nanoparticles, offers an attractive platform for an efficient control of light–matter interaction in various nanoscale functional photonic elements and devices, including broadband absorbers, efficient nonlinear light sources, nanolasers, and ultrasensitive biosensors. Novel horizons in applications driven by the controllable anapole response, such as noninvasive sensing, broadband photodetectors, near-field lasing, spurious scattering suppression, and optical invisibility, can be explored in the near future in all-dielectric resonant photonics.

Acknowledgements

The authors acknowledge useful suggestions and comments from A. Basharin, A. Evlyukhin, A. Fratalocchi, and Wei Liu, and they are also thankful to all colleagues and co-authors of joint papers for valuable contributions. The work was supported by the Government of the Russian Federation (Grant 08-08), the Ministry of Science and Higher Education of the Russian Federation (project No. 16.12780.2018/12.2), the Russian Foundation for Basic Research (Grant 18-02-00381), the Australian Research Council, and the Strategic Fund of the Australian National University. The studies on anapole metamaterials were supported by the Russian Science Foundation (project 17-72-10230). B.S.L. also acknowledges support by the Russian Ministry of Education and Science (#14.W03.31.0008).

Conflict of Interest

The authors declare no conflict of interest.

Keywords

anapole mode, metaoptics, metasurfaces, Mie resonances, nanophotonics

Received: October 4, 2018
Revised: November 30, 2018
Published online:

[1] N. Papasimakis, V. A. Fedotov, V. Savinov, T. A. Raybould, N. I. Zheludev, *Nat. Mater.* **2016**, *15*, 263.
[2] D. Smirnova, Y. S. Kivshar, *Optica* **2016**, *3*, 1241.
[3] C. F. Bohren, D. R. Huffman, *Absorption and Scattering of Light by Small Particles*, Wiley, New York **1983**.
[4] J. Jackson, *Classical Electrodynamics*, Wiley, New York **1999**.
[5] P. Grahn, A. Shevchenko, M. Kaivola, *New J. Phys.* **2012**, *14*, 093033.
[6] E. E. Radescu, G. Vaman, *Phys. Rev. E* **2002**, *65*, 046609.
[7] I. Zeldovich, *J. Exp. Theor. Phys.* **1957**, *33*, 1531.
[8] C. S. Wood, S. C. Bennett, D. Cho, B. P. Masterson, J. L. Roberts, C. E. Tanner, C. E. Wieman, *Science* **1997**, *275*, 1759.
[9] C. M. Ho, R. J. Scherrer, *Phys. Lett. B* **2013**, *722*, 341.
[10] Y. Gao, C. M. Ho, R. J. Scherrer, *Phys. Rev. D* **2014**, *89*, 045006.
[11] A. B. Evlyukhin, C. Reinhardt, A. Seidel, B. S. Luk'yanchuk, B. N. Chichkov, *Phys. Rev. B* **2010**, *82*, 045404.
[12] A. B. Evlyukhin, C. Reinhardt, B. N. Chichkov, *Phys. Rev. B* **2011**, *84*, 235429.
[13] A. E. Miroshnichenko, A. B. Evlyukhin, Y. F. Yu, R. M. Bakker, A. Chipouline, A. I. Kuznetsov, B. Luk'yanchuk, B. N. Chichkov, Y. S. Kivshar, *Nat. Commun.* **2015**, *6*, 1.
[14] B. Luk'yanchuk, R. Paniagua-Domínguez, A. I. Kuznetsov, A. E. Miroshnichenko, Y. S. Kivshar, *Phys. Rev. A* **2017**, *95*, 063820.
[15] R. Alaee, C. Rockstuhl, I. Fernandez-Corbaton, *Adv. Optical Mater.* **2019**, *7*, 1800783.
[16] S.-Q. Li, K. B. Crozier, *Phys. Rev. B* **2018**, *97*, 245423.
[17] P. C. Wu, C. Y. Liao, V. Savinov, T. L. Chung, W. T. Chen, Y.-W. Huang, P. R. Wu, Y.-H. Chen, A.-Q. Liu, N. I. Zheludev, D. P. Tsai, *ACS Nano* **2018**, *12*, 1920.
[18] N. A. Butakov, J. A. Schuller, *Sci. Rep.* **2016**, *6*, 1.
[19] M. Born, E. Wolf, *Principles of Optics*, 7th ed., Cambridge University Press, Cambridge, UK **1999**.
[20] B. Luk'yanchuk, R. Paniagua-Domínguez, A. I. Kuznetsov, A. E. Miroshnichenko, Y. S. Kivshar, *Philos. Trans. R. Soc. A* **2017**, *375*, 20160069.
[21] V. Savinov, *Phys. Rev. A* **2018**, *97*, 063834.
[22] B. Luk'yanchuk, N. I. Zheludev, S. A. Maier, N. J. Halas, P. Nordlander, H. Giessen, C. T. Chong, *Nat. Mater.* **2010**, *9*, 707.
[23] B. S. Luk'yanchuk, N. V. Voshchinnikov, R. Paniagua-Domínguez, A. I. Kuznetsov, *ACS Photonics* **2015**, *2*, 993.
[24] A. B. Evlyukhin, T. Fischer, C. Reinhardt, B. N. Chichkov, *Phys. Rev. B* **2016**, *94*, 205434.
[25] P. D. Terekhov, K. V. Baryshnikova, Y. A. Artemyev, A. Karabchevsky, A. S. Shalin, A. B. Evlyukhin, *Phys. Rev. B* **2017**, *96*, 035443.
[26] V. A. Zenin, A. B. Evlyukhin, S. M. Novikov, Y. Yang, R. Malureanu, A. V. Lavrinenko, B. N. Chichkov, S. I. Bozhevolnyi, *Nano Lett.* **2017**, *17*, 7152.
[27] E. A. Gurvitz, K. S. Ladutenko, P. A. Dergachev, A. B. Evlyukhin, A. E. Miroshnichenko, A. S. Shalin, *arXiv:1810.04945*, **2018**.
[28] S. Nanz, *Toroidal Multipole Moments in Classical Electrodynamics*, Springer Fachmedien Wiesbaden, Wiesbaden **2016**.
[29] V. Dubovik, V. Tugushev, *Phys. Rep.* **1990**, *187*, 145.
[30] N. A. Nemkov, A. A. Basharin, V. A. Fedotov, *Phys. Rev. B* **2017**, *95*, 165134.
[31] N. A. Nemkov, A. A. Basharin, V. A. Fedotov, *Phys. Rev. A* **2018**, *98*, 023858.
[32] B. Stout, R. McPhedran, *Europhys. Lett.* **2017**, *119*, 44002.
[33] D. A. Powell, *Phys. Rev. Appl.* **2017**, *7*, 034006.
[34] J. S. T. Gongora, G. Favraud, A. Fratalocchi, *Nanotechnology* **2017**, *28*, 104001.
[35] T. Kaelberer, V. A. Fedotov, N. Papasimakis, D. P. Tsai, N. I. Zheludev, *Science* **2010**, *330*, 1510.
[36] V. A. Fedotov, A. V. Rogacheva, V. Savinov, D. P. Tsai, N. I. Zheludev, *Sci. Rep.* **2013**, *3*, 1.
[37] A. Sayanskiy, M. Danaeifar, P. Kapitanova, A. E. Miroshnichenko, *Adv. Opt. Mater.* **2018**, 1800302.
[38] L. Cong, V. Savinov, Y. K. Srivastava, S. Han, R. Singh, *Adv. Mater.* **2018**, 1804210.
[39] N. Talebi, S. Guo, P. A. van Aken, *Nanophotonics* **2018**, *7*, 93.
[40] L.-Y. Guo, M.-H. Li, X.-J. Huang, H.-L. Yang, *Appl. Phys. Lett.* **2014**, *105*, 033507.
[41] M. Li, L. Guo, J. Dong, H. Yang, *Appl. Phys. Express* **2014**, *7*, 082201.
[42] H.-m. Li, S.-b. Liu, S.-y. Liu, S.-y. Wang, G.-w. Ding, H. Yang, Z.-y. Yu, H.-f. Zhang, *Appl. Phys. Lett.* **2015**, *106*, 083511.
[43] W. Liu, J. Zhang, A. E. Miroshnichenko, *Laser Photonics Rev.* **2015**, *9*, 564.
[44] A. A. Basharin, V. Chuguevsky, N. Volsky, M. Kafesaki, E. N. Economou, *Phys. Rev. B* **2017**, *95*, 035104.
[45] N. A. Nemkov, I. V. Stenishchev, A. A. Basharin, *Sci. Rep.* **2017**, *7*, 1.
[46] W. Liu, J. Zhang, B. Lei, H. Hu, A. E. Miroshnichenko, *Opt. Lett.* **2015**, *40*, 2293.
[47] L. Wei, Z. Xi, N. Bhattacharya, H. P. Urbach, *Optica* **2016**, *3*, 799.
[48] W. Liu, J. Zhang, B. Lei, H. Hu, A. E. Miroshnichenko, *Opt. Lett.* **2015**, *40*, 2293.
[49] W. Liu, B. Lei, J. Shi, H. Hu, A. E. Miroshnichenko, *J. Nanomater.* **2015**, *2015*, 672957.
[50] W. Liu, J. Shi, B. Lei, H. Hu, A. E. Miroshnichenko, *Opt. Express* **2015**, *23*, 24738.
[51] A. G. Lamprianidis, A. E. Miroshnichenko, *Beilstein J. Nanotechnol.* **2018**, *9*, 1478.
[52] J. Tian, H. Luo, Y. Yang, Y. Qu, D. Zhao, M. Qiu, S. I. Bozhevolnyi, *arXiv:1807.11015*, **2018**.
[53] Y. Yang, V. A. Zenin, S. I. Bozhevolnyi, *ACS Photonics* **2018**, *5*, 1960.
[54] G. Grinblat, Y. Li, M. P. Nielsen, R. F. Oulton, S. A. Maier, *Nano Lett.* **2016**, *16*, 4635.
[55] T. Shibanuma, G. Grinblat, P. Albella, S. A. Maier, *Nano Lett.* **2017**, *17*, 2647.
[56] V. F. Gili, L. Ghirardini, D. Rocco, G. Marino, I. Favero, I. Roland, G. Pellegrini, L. Duò, M. Finazzi, L. Carletti, A. Locatelli,

A. Lemaître, D. Neshev, C. De Angelis, G. Leo, M. Celebrano, *Beilstein J. Nanotechnol.* **2018**, *9*, 2306.
[57] G. Grinblat, Y. Li, M. P. Nielsen, R. F. Oulton, S. A. Maier, *ACS Nano* **2016**, *11*, 953.
[58] M. Timofeeva, L. Lang, F. Timpu, C. Renaut, A. Bouravleuv, I. Shtrom, G. Cirlin, R. Grange, *Nano Lett.* **2018**, *18*, 3695.
[59] L. Xu, M. Rahmani, K. Z. Kamali, A. Lamprianidis, L. Ghirardini, J. Sautter, R. Camacho-Morales, H. Chen, M. Parry, I. Staude, G. Zhang, D. Neshev, A. E. Miroshnichenko, *Light: Sci. Appl.* **2018**, *7*, 1.
[60] J. S. T. Gongora, A. E. Miroshnichenko, Y. S. Kivshar, A. Fratalocchi, *Nat. Commun.* **2017**, *8*, 15535.
[61] D. Rocco, V. F. Gili, L. Ghirardini, L. Carletti, I. Favero, A. Locatelli, G. Marino, D. N. Neshev, M. Celebrano, M. Finazzi, G. Leo, C. D. Angelis, *Photonics Res.* **2018**, *6*, B6.
[62] D. G. Baranov, R. Verre, P. Karpinski, M. Käll, *ACS Photonics* **2018**, *5*, 2730.
[63] M. A. Noginov, G. Zhu, A. M. Belgrave, R. Bakker, V. M. Shalaev, E. E. Narimanov, S. Stout, E. Herz, T. Suteewong, U. Wiesner, *Nature* **2009**, *460*, 1110.
[64] Y.-J. Lu, J. Kim, H.-Y. Chen, C. Wu, N. Dabidian, C. E. Sanders, C.-Y. Wang, M.-Y. Lu, B.-H. Li, X. Qiu, W.-H. Chang, L.-J. Chen, G. Shvets, C.-K. Shih, S. Gwo, *Science* **2012**, *337*, 450.
[65] M. H. Huang, *Science* **2001**, *292*, 1897.
[66] R. Chen, T.-T. D. Tran, K. W. Ng, W. S. Ko, L. C. Chuang, F. G. Sedgwick, C. Chang-Hasnain, *Nat. Photonics* **2011**, *5*, 170.
[67] J. S. T. Gongora, A. E. Miroshnichenko, Y. S. Kivshar, A. Fratalocchi, *CLEO: QELS Fundamental Science (CLEO_QELS 2016)*, OSA Publishing, Washington **2016**, p. FTh3A7.
[68] *Integrated Optics: Devices, Materials, and Technologies XXI* (Eds: J. S. T. Gongora, A. E. Miroshnichenko, Y. S. Kivshar, A. Fratalocchi, S. M. García-Blanco, G. N. Conti), SPIE, **2017**.
[69] S.-D. Liu, Z.-X. Wang, W.-J. Wang, J.-D. Chen, Z.-H. Chen, *Opt. Express* **2017**, *25*, 22375.
[70] V. Mazzone, J. T. Gongora, A. Fratalocchi, *Appl. Sci.* **2017**, *7*, 542.
[71] A. K. Ospanova, I. V. Stenishchev, A. A. Basharin, *Laser Photonics Rev.* **2018**, *12*, 1800005.
[72] A. K. Ospanova, G. Labate, L. Matekovits, A. A. Basharin, *Sci. Rep.* **2018**, *8*, 12514.
[73] T. Feng, Y. Xu, W. Zhang, A. E. Miroshnichenko, *Phys. Rev. Lett.* **2017**, *118*, 17.
[74] K. Baryshnikova, D. Filonov, C. Simovski, A. Evlyukhin, A. Shalin, in *2017 Progress in Electromagnetics Research Symp.—Spring (PIERS)*, (Eds: W. C. Chew, S. He), IEEE Xplore **2017**, pp. 2813–2816.
[75] P. D. Terekhov, K. V. Baryshnikova, A. S. Shalin, A. B. Evlyukhin, I. A. Khromova, *Days on Diffraction (DD)*, OSA, **2016**, pp. 406–409.
[76] M. V. Cojocari, A. A. Basharin, in *Advanced Photonics 2018 (BGPP, IPR, NP, NOMA, Sensors, Networks, SPPCom, SOF)*, Part "Novel Optical Materials and Applications", OSA Publishing, Washington **2018**, p. NoW1D.4.
[77] R. Wang, L. D. Negro, *Opt. Express* **2016**, *24*, 19048.
[78] J. Wang, N. Wang, J. Hu, R. Jiang, *Opt. Express* **2017**, *25*, 28935.
[79] H. Shamkhi, K. Baryshnikova, P. K. A. Sayanskiy, P. Terekhov, P. Belov, A. Karabchevsky, A. Evlyukhin, Y. Kivshar, A. Shalin, *arXiv:1808.10708v1*, **2018**.
[80] M. Rybin, K. Koshelev, Z. Sadrieva, K. S. A. Bogdanov, M. Limonov, Y. Kivshar, *Phys. Rev. Lett.* **2017**, *119*, 243901.
[81] W. Chen, Y. Chen, W. Liu, *arXiv:1808.05539v1*, **2018**.
[82] S.-D. Liu, J.-L. Fan, W.-J. Wang, J.-D. Chen, Z.-H. Chen, *ACS Photonics* **2018**, *5*, 1628.
[83] M. Kerker, D.-S. Wang, C. L. Giles, *J. Opt. Soc. Am. B* **1983**, *73*, 765.
[84] W. Liu, Y. S. Kivshar, *Opt. Express* **2018**, *26*, 13085.
[85] A. Poddubny, D. Smirnova, *arXiv:1808.04811v1*, **2018**.
[86] L. Carletti, K. Koshelev, C. D. Angelis, Y. Kivshar, *Phys. Rev. Lett.* **2018**, *121*, 033903.